Photoresponsive Hydrogel Microcrawlers Exploit Friction Hysteresis to Crawl by Reciprocal Actuation.

I. Rehor[1,4,5], C. Maslen[1,4], P. G. Moerman[1], B. G. P van Ravensteijn[2], R. van Alst[1], J. Groenewold[1,6], H. B. Eral[1,3,*], W. K. Kegel[1,*]

Affiliations

1 Van 't Hoff Laboratory for Physical and Colloid Chemistry, Debye Institute for Nanomaterials Science, Utrecht University, The Netherlands.

2 Netherlands Organization for Applied Scientific Research (TNO), Materials Solutions, High Tech Campus 5, 5656 AE Eindhoven, The Netherlands.

3 Process & Energy Laboratory, 3ME Faculty, TU Delft, The Netherlands

4 Faculty of Chemical Engineering, UCT Prague

5 IOCB, Prague, Czech Republic

6 Guangdong Provincial Key Laboratory of Optical Information Materials and Technology & Institute of Electronic Paper Displays, South China Academy of Advanced Optoelectronics, South China Normal University, Guangzhou 510006, China

*Correspondence to w.k.kegel@uu.nl and h.b.eral@tudelft.nl

Abstract

Mimicking the locomotive abilities of living organisms on the microscale, where the downsizing of rigid parts and circuitry presents inherent problems, is a complex feat. In nature, many soft-bodied organisms (inchworm, leech) have evolved simple, yet efficient locomotion strategies in which reciprocal actuation cycles synchronize with spatiotemporal modulation of friction between their bodies and environment. In this research, microscopic (100 μm) hydrogels are demonstrated to crawl in an aqueous environment by reciprocal actuation coupled to spatiotemporal modulation of friction between the gel and the surface. Thermo-responsive poly-n-isopropyl acrylamide hydrogels loaded with gold nanoparticles shrink locally and reversibly when heated photothermally with laser light. Off-center irradiation of the hydrogel combined with hysteresis in the friction of the gel between shrinking and expanding cycles results in a crawling motion. We show that microcrawlers are steerable and can push small cargo along a surface.

Main Text

Introduction

Miniaturization of untethered mobile robots toward the micron-scale can enable their application in currently problematic tasks such as parallel micromanipulation, drug delivery and microsurgery.[1–5] Multiple approaches for untethered microrobot powering and driving are currently under investigation. One approach is to directly manipulate the microrobot by external magnetic[6–8] or electric field.[9] An alternative approach is to produce microrobots that can locomote through the mechanical interactions of their bodies to their surroundings by propulsion or mechanical actuation.

In such cases, the forces responsible for locomotion are localized to the microrobot and, thus, these methods do not, in principle, require any external set-up which holds the most promise for fully autonomous systems and in the field applications.[10] The locomotion provided by mechanical actuation provides robust and variable motility (jumping,[11] crawling,[12–15] swimming[16–18]) in both wet and dry environments. The energy required for actuation can be provided by biological actuators,[19] or can be directly harvested from the environment as chemical energy[20,21] or electromagnetic radiation. Transducing visible light into mechanical actuation has been widely adopted as a practical method of powering remote untethered microrobots.[22] Such robots are typically constructed from photoresponsive soft materials that respond to irradiation by shape or volumetric changes.[23–29] Two classes of soft photoresponsive materials have been predominantly used for microrobot construction: liquid crystal elastomers (LCEs) and thermoresponsive hydrogels - made photoresponsive by incorporating highly absorptive materials.[30] In this work, we use the latter.

Actuating microrobots undergo changes in their volume or shape in repetitive cycles, strokes, to exert frictional forces to a substrate (crawlers) or viscous forces to a surrounding media (swimmers). The robot must exert this force along a certain distance to perform mechanical work and, thus displace. The shape changes it undergoes are cyclic and, thus, a symmetry breaking phenomenon must be present to keep the mechanical work non-zero over the course of the entire cycle.[31,32] In the absence of inertia,[33,34] this symmetry breaking is typically realized experimentally by inducing non-reciprocal shape changes. A disadvantage of non-reciprocal actuation is that it requires a larger complexity – at least two degrees of freedom actuation[35] which hinders miniaturization,[23,27] large scale production, and independent control over multiple robots.[23]

In the case of crawlers, single degree of freedom reciprocal actuation such as bending in an inchworm fashion[20,36–38] or isotropic contraction-expansion[24] may also provide directional motion when coupled to a head-to-tail asymmetry in friction with the surface. Such friction asymmetry can come from angled bristles[24,39] or ratcheted surfaces.[8,14,20,40] Reciprocal actuation is much simpler to realize than non-reciprocal actuation, so this route holds promise for upscaling the production of independently controlled miniature robots. However, thus far the manufacture of angled bristles does not allow massive production of miniature robots and the requirement of surface texturing has stood in the way of their omnidirectional control.[24]

In this work, we developed photoresponsive hydrogel crawlers of approximately 100 µm locomoting in aqueous environments being powered and steered by pulses of focused light. We show that these microcrawlers can move by reciprocal actuation without the requirement of surface texturing. Instead, the friction coefficient between the microcrawler and the substrate changes

asymmetrically over the course of one contraction-expansion cycle, resulting in the microcrawler's directional motion. We developed a model based on the concept of synchronized actuation and friction modulation that reproduced experimental data, without adjustable parameters. We then constructed a steerable microcrawler with the ability to manipulate and assemble other objects.

Materials and Methods

N-isopropylacrylamide (NIPAM), poly(ethylene glycol) diacrylate (PEGDA, average Mn = 700 kDa), trisodium citrate, polyvinylpyrrolidone (PVP, Mw = 360 kDa), Tween 20, and Pluronic F127 were purchased from Sigma Aldrich. Tetrachloroaurate trihydrate ($HAuCl_4 \cdot 3H_2O$) was purchased from Alfa Aesar. Methacryloxyethyl thiocarbamoyl Rhodamine B was obtained from Polysciences. SYLGARD® 184 silicone elastomer kit (elastomer base + curing agent), used for the fabrication of polydimethylsiloxane (PDMS) microfluidic channels, was purchased from Dow Corning. All chemicals were purchased in standard purities provided by the vendors and used as received. The photo-initiator lithium phenyl-2,4,6-trimethylbenzoylphosphinate (LAP) was synthesized according to a previously published procedure.[41] Reverse osmosis water (MilliQ) was used for all experiments (18.2 MΩ at 25 °C).

Microcrawler Synthesis

100 µL 1-1.5 % w/w gold nanoparticles dispersion (synthesized using citrate method - see supplementary methods) was mixed with NIPAM (37 mg, 327 µmol), PEGDA (20 µL, 29 µmol) and LAP (1.5 mg, 5 µmol). The mixture was sonicated for 5 min to dissolve the components. The pre-gel solution was always used the same day and centrifuged before use to remove dust and gold colloid agglomerates (2 min at 5000 rcf). Hydrogel cubes for the steering experiment were synthesized using SFL and consist of pure PEGDA crosslinked using 1 % (w/w) LAP.

To produce hydrogel microcrawlers, the resulting mixture was processed in stop-flow lithography, which was performed as previously described (details on the procedure are in the supplementary methods).[42] After synthesis (typically several thousand microcrawlers were prepared in one run), the channel was purged with 0.5% aqueous Tween 20 solution (150 µL) and the microcrawlers were collected inside a PCR tube. The dispersion of microcrawlers was washed with Tween 20 solution 4 times, being allowed to sediment under gravity for 5 min between each washing step. The Tween 20 prevents the microcrawlers to stick irreversibly to each other and to the container surface.

Crawling

Glass microscope slides (Menzel) were spin-coated with PDMS (volume ratio base : curing agent = 10 : 1). Subsequently, plastic washers (inner diameter 10 mm, height 2 mm) were placed on the glass slide and the whole assembly was cured overnight at 65 °C. The prepared wells were filled with microcrawlers dispersed in 0.5% (w/w) Tween 20 aqueous solution. The wells were covered with a glass slide and sealed using UV-curable adhesive.

A 200 mW diode laser (532 nm) was attenuated using a grey filter (optical density = 0.5) and placed directly inside the condenser of an inverted microscope (Nikon Ti-U). The condenser was used to focus the laser beam to the sample plane. Four white LEDs were fixed around the laser collimating lens to illuminate the sample for bright-field microscopy. A picture of the setup can be found in figure S3. The sample well with microcrawlers was placed under the inverted microscope with the laser setup installed. The laser beam was aimed at a particular part of the microcrawler and laser pulses (0.5–0.7 s on, 1–1.5 s off) were applied. A 536 nm short pass filter was placed underneath the sample and a cube filter for RITC (Semrock) was placed in the light path, both to block the laser beam and allow diascopic observation of irradiated microcrawlers.

The crawling experiments were performed on three alternative surfaces to the nominal PDMS, namely bare glass, C18 hydrophobized glass, and perfluorated C8 coated glass. Both glass coatings were performed by vapor deposition: the glass slide was immersed in 1 M NaOH for 1 hour, then washed with water, dried with a stream of air and placed inside a desiccator together with 300 µL of trichloro(octadecyl)silane and trichloro(1H,1H,2H,2H-perfluorooctyl)silane respectively and left at 40 mBar for 2 hours.

Sliding Experiments

A glass capillary (50 × 5 × 0.5 mm) was filled with PDMS (volume ratio base : curing agent : toluene = 10 : 1 : 10), and spin coated horizontally (2000 RPM, 1 min) to coat its inner surface. After curing, the capillary was filled with a 0.5% Tween 20 solution containing approximately 30 disc-shaped microcrawlers (diameter = 115 µm) and sealed using UV curable glue. The capillary was placed on a heating stage (Linkam) attached to the sample holder of a Nikon LV100Pol microscope equipped with a DMK23ux174 camera imaging a plane parallel to gravity. The setup detail is depicted in Figure S4. The capillary was then tilted by 10° to induce the sliding of the microcrawlers. Simultaneously the stage was repetitively heated to 65 °C and cooled back to 25 °C at 20 °C/min. The microcrawler sizes and sliding velocities were measured manually and averaged over 5 individual experiments.

Results

Microcrawler Synthesis and Locomotion

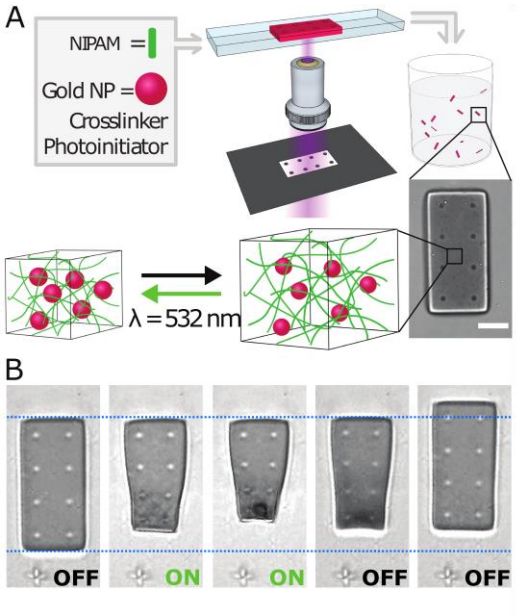

Fig. 1. Microcrawler synthesis and actuation. A – Microcrawlers are synthesized inside a microfluidic channel using stop-flow lithography. Scale bar is 20 µm. Hydrogels consist of thermoresponsive PNIPAM with entrapped AuNPs. Absorption of green light by AuNPs raises the local temperature above PNIPAM's lower critical solution temperature, resulting in shrinkage. B – Individual crawling stages, with indicated on and off irradiation periods. A microcrawler is irradiated off-center with focused green light pulses. The irradiated area contracts and expands periodically, resulting in the forward motion of the entire microcrawler.

Microcrawlers (100 × 50 × 30 µm) were synthesized using stop-flow lithography (SFL), a high throughput lithographic technique that enables the production of microscale hydrogels with 2D geometries defined by a photomask (Figure 1A).[42] They are composed of poly(N-isopropylacrylamide) (PNIPAM) crosslinked with poly(ethylene glycol) diacrylate (PEGDA) and contain 15 nm gold nanoparticles (AuNPs) entrapped in the hydrogel network. The microcrawlers sedimented in aqueous environments under gravity and their motion along the surface was induced by pulses of focused green laser irradiation (λ = 532 nm). The surface plasmon resonance of 15 nm AuNPs has a wavelength of 520 nm which is sufficiently close to the laser wavelength to enable plasmonic absorption. The energy is dissipated as heat to the surrounding network which causes reversible shrinkage of the thermo-responsive PNIPAM. Pulsed laser light (typically 0.7 s on, 1.3 s off) induced periodic reciprocal contraction and expansion cycles, localized to the irradiated section of the microcrawler. After each cycle, the microcrawler moved away from the center of irradiation (Figure 1B). This motion was observed on multiple surfaces including glass, hydrophobized glass and spin-coated PDMS (supplementary information S1). On the PDMS surface, the crawler moved the furthest – approximately 15 µm per cycle – so this surface was used throughout the rest of the study.

The actuation of the microcrawler was reciprocal; from top view, the pathway of its shape change during contraction was identical to that during expansion (Figure 1B). It was shown in multiple theoretical studies, that reciprocal actuation in the absence of inertia (The Reynolds number in our system is on the order of 10^{-3}) does not cause net displacements, unless another form of symmetry breaking is provided.[32,35,38,43] We found that the microcrawler undergoes a cycle of high friction during expansion and low friction during contraction. This friction modulation synchronized to the reciprocal actuation breaks the symmetry of the forces in each stroke.

Microcrawler Friction Hysteresis

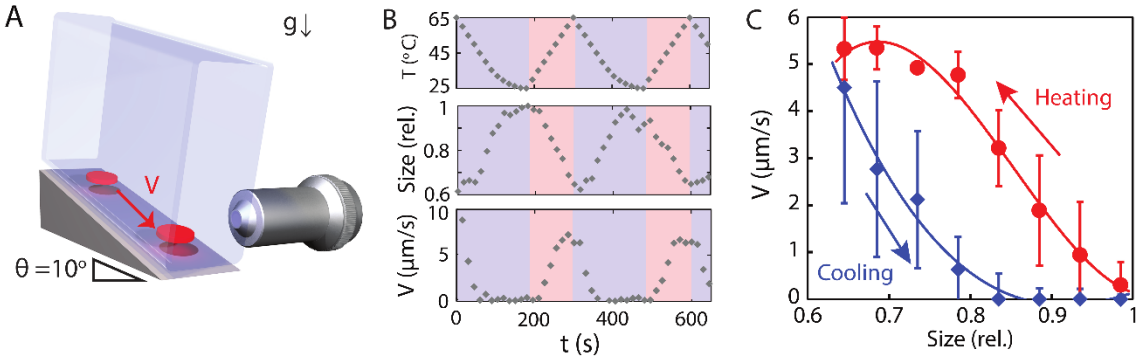

Fig. Figure 2. Sliding experiments and friction hysteresis. A – Disc-shaped hydrogels placed in a tilted capillary were exposed to heating/cooling cycles. Their gravity-induced sliding velocity, V was observed. B – Temperature of the heating stage, T, relative disk size and the sliding velocity. C –The sliding velocity increases with hydrogel contraction during heating (red circles) and cooling (blue diamonds), forming a hysteresis loop.

To investigate the friction between the microcrawler and the substrate, we performed a series of experiments with microcrawlers sliding over a tilted surface under the influence of gravity (figure 2A). Microcrawlers were sealed inside a tilted glass capillary and observed from the side using a microscope. We chose disc-shaped microcrawlers for these experiments as their observed cross-section from the side is invariant to their orientation on the plane. At constant temperature, the discs slide at constant velocity down the slope (Figure S5). Discs on the tilted plane are subjected to the lateral component of the gravitational force (F_l) which is a function of the net mass with respect to the surrounding fluid (m) and tilt angle (ϑ). For a sliding hydrogel we will define the dynamic friction coefficient (f) per unit area[44,45]:

$$F_{fr} = S\, f\, v \qquad [1]$$

With v the sliding velocity, S the area of the hydrogel disc and F_{fr} the friction force (tangential to the substrate). During the sliding experiments with the hydrogel discs, we assume inertial effects and

the viscous drag to be negligible (justification in S2), therefore friction constant can be obtained by equating the frictional force to the gravity force component parallel to the substrate. This gives the following expression for the normalised friction constant from the tilt angle and the buoyant mass m of the disc:

$$f = \frac{m\, g\, \sin\vartheta}{S\, v} \qquad [2]$$

Thus, from the terminal sliding velocity of the hydrogel discs, one can calculate the normalized friction coefficient as a function of the size of the disc, or equivalently, the state of contraction.

To mimic the conditions in the irradiated area of the microcrawler, the disc suspension was exposed to heating and cooling cycles. Upon heating, the discs shrunk and accelerated. During the cooling process, the discs swelled and decelerated again, but instead of regaining their original speed they fully stopped and stuck to the capillary wall, indicating the friction force outcompeted the lateral component of the gravitational force. Upon reheating, the discs shrunk and started moving again. The temperature, speed, and size of one sliding disc are plotted as function of time for consecutive heating-cooling cycles in Figure 2B. To show that the friction coefficient of hydrogels in the same degree of swelling is different during contraction than during expansion, we plotted the sliding velocity as a function of particle size (Figure 2C). The plot exhibits a clear hysteresis: the friction coefficient is lower during contraction than during expansion (eq. 2).

The friction hysteresis shown in Figure 2C is responsible for the net displacement of microcrawlers away from the irradiation spot. When one side of a microcrawler is heated as a consequence of laser irradiation, the friction of the irradiated part of the hydrogel with the surface is smaller than the friction of the other side of the hydrogel with the surface. As a consequence, the center of contraction (i.e. the point of the crawler not displacing with respect to the substrate) of the hydrogel is not the center of mass, but rather a point further from the irradiated side. Inversely, after the laser is turned off, the previously irradiated section swells and has higher friction with the surface than the other side. This causes the center of expansion to be closer to the irradiated side of the hydrogel. This mismatch between the center of contraction and the center of expansion causes the crawlers to move away from the laser beam.

We ascribe the observed friction hysteresis to the previously described hysteresis in the surface states of PNIPAM during shrinking and swelling cycles. PNIPAM hydrogels display such hysteresis when either swelling or de-swelling rapidly, i.e. out of equilibrium. During fast shrinkage, water is ejected faster from the surface of the gel than the inner material, forming a dense surface layer (often called

'skin').[46,47] During cooling the outer layer expands first and promotes reswelling by elastic stress. This out-of-equilibrium behavior has been previously exploited for complex shape changes of a PNIPAM gel during shrinking and expanding cycles to produce a non-reciprocally actuating microswimmer.[18] Multiple studies, focusing on out-of-equilibrium collapse and reswelling of PNIPAM brushes, brought insight to the underlying processes on the molecular level.[48–53] In the collapsed state, new interactions between individual PNIPAM chains are established (hydrogen bonds,[51] entanglement[52]). During re-swelling, these interactions are being broken which imposes extra energy barriers on the swelling process that were not present during the collapse. These kinetic barriers change the energy landscape of the re-swelling process and therefore the swelling polymer chain is undergoing a different pathway of consecutive conformational changes to reestablish its original volume.[48,49] It was described, that these conformational differences result in different topography between swelling and shrinking polymer brushes.[48] We conclude that this topographical difference between collapsing and expanding PNIPAM hydrogel is responsible for our observations of friction hysteresis.

An additional contribution to the friction hysteresis could come from hysteresis in the lubricating layer thickness between the microcrawler and the surface. After sedimentation, the microcrawler is separated from the substrate by a thin layer of solvent.[44,45] As the microcrawler is heated, water is expelled which thickens the lubrication layer and reduces the friction locally. Because the hydrogel has a positive net mass, it sediments towards the substrate and re-establishes the equilibrium lubrication layer. We measured the change in velocity of discs that were sliding down a slope during and after heating. Their sliding velocity peaks during heating and then slows down to an equilibrium value, consistent with the idea that an equilibrium lubrication layer re-establishes after the contraction is complete (Figure S7). During the subsequent expansion phase, water is reabsorbed into the gel, reducing the lubrication layer thickness.[54]

To directly show that the friction hysteresis is responsible for the directional crawling, we repeated both crawling and sliding experiments in a Pluronic surfactant solution. Pluronic strongly adsorbs onto the PDMS surface[55] and lubricates it which reduces the friction between the surface and the crawler.[56] The friction reduction can be observed in the sliding experiments; the sliding velocity of hydrogels in the same degree of swelling differs much less between contraction and expansion (Figure S8) than in the case of the Tween. Moreover, the hydrogels do not stop moving during the cooling phase. The small friction hysteresis in a heating-cooling cycle suggests that crawling should be inefficient in presence of pluronic surfactant, and indeed, the observed net displacement per cycle was only 1 to 2 µm compared to 15 µm in absence of surfactant. We conclude that the surface lubrication by pluronic suppresses the friction hysteresis which results in the loss of displacement.

Microcrawler model

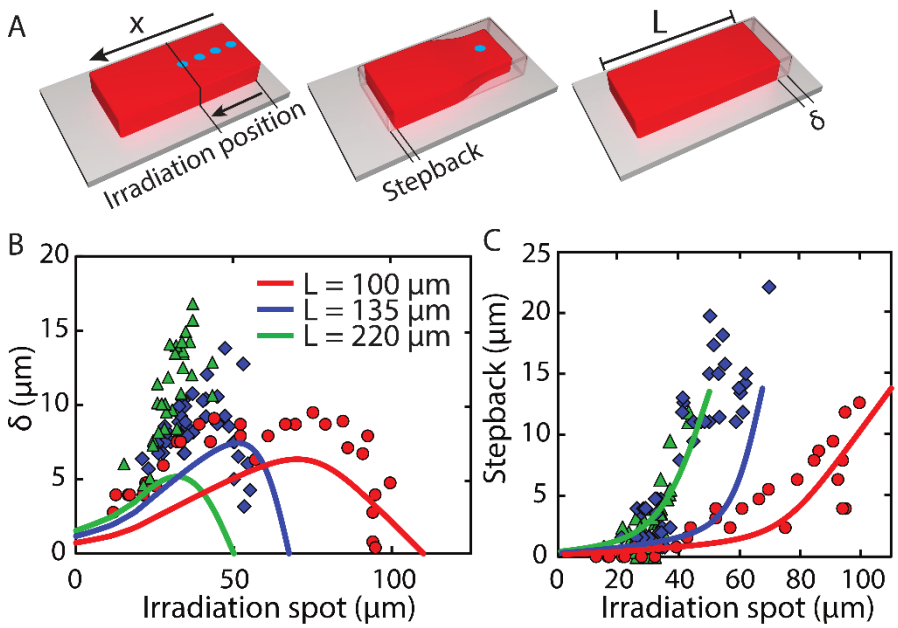

Figure 3. Step size variation with irradiation position and microcrawler size. A – Cartoon of rectangular microcrawler indicating the relevant geometrical parameters. B and C – Net displacement and stepback as a function of irradiation position for 100 μm (Δ), 135 μm (◊) and 220 μm (○) microcrawlers. Solid lines were calculated with no adjustable parameters from Eq. 1 (detailed description in SI)

To get quantitative insight into the crawling mechanism, we conducted a series of crawling experiments with rectangular microcrawlers of constant height and width (25 × 50 μm), but differing in length (100, 135 and 220 μm). The net displacement (δ) achieved in an individual stroke as a function of the center of the irradiation spot along the main microcrawler axis (Fig. 3A) was examined for this series of microcrawlers (Fig. 3B) with pulses of 0.7s. The initial increase in the net displacement that occurs as the laser beam center moves from the rear edge towards the center is ascribed to the increase of the irradiated part of the microcrawler (beam has a finite diameter), which results in increasing length difference between contracted and expanded microcrawler. This length difference determines the amplitude of the microcrawler actuation and therefore the magnitude of the net displacement. However, when the beam center approaches the geometric center of the particle, the head-tail asymmetry of the microcrawler is lost and the net displacement drops again. This symmetry constraint can also be observed as the distance by which the front, non-actuating, end of the microcrawler retracts ('stepback') during the contraction phase (Fig. 3C). When the beam is sufficiently far from the center, the front section of the microcrawler serves as an anchor and the contracting section with its reduced friction with the substrate is not capable to pull it backward during contraction. When the beam is placed closer to the center of the particle, the difference in friction forces exerted by the front and the rear part of the microcrawler is diminishing and the step back

increases. When the microcrawler is irradiated in the middle, the step back is equal to one half of the total contracted length and the resulting net stroke is zero (an example of symmetric irradiation is in Movie S4).

We constructed a model that utilizes the observed hysteresis in the friction of the sliding gel-discs to predict the net displacement (δ) for rectangular microcrawlers irradiated at designated positions (full derivation in supplementary information section S3). In a cycle of expansion and contraction, δ is achieved as a result of hysteresis (eq. 3).

$$\delta = \int_0^{\varepsilon_{\max}} d\varepsilon \frac{\partial x_0}{\partial \varepsilon}\Big|_{\text{contraction}} + \int_{\varepsilon_{\max}}^{0} d\varepsilon \frac{\partial x_0}{\partial \varepsilon}\Big|_{\text{expansion}}$$

$$\delta = \int_0^{\varepsilon_{max}} d\varepsilon \frac{\partial x_0}{\partial \varepsilon}\Big|_{contraction} + \int_{\varepsilon_{max}}^{0} d\varepsilon \frac{\partial x_0}{\partial \varepsilon}\Big|_{expansion} \quad [3]$$

In this expression, the position of the rear end of the crawler, $x_{0,}$ is a function of the relative deformation ε with respect to the swollen state. Where ε is the relative contraction in width of the crawler evaluated at the center of the irradiation spot. ε is a function of time and its maximum value, at the end of the heating part of the cycle, is denoted by ε_{max}. Due to the hysteresis in friction, the rear end position as a function of contraction is dependent on whether it takes place in the heating or the cooling cycle. Therefore, the expansion term does not cancel the contraction term, which results in a net displacement. To get a more explicit description for the crawling motion a semi-empirical model has been developed (details to be found in Supplementary Information section S3). Inputs for this model are the normalized friction coefficients obtained from the sliding discs on the tilted substrate. Further, the model assumptions are as follows: it is assumed that the sliding stress on the substrate and crawler is varying as a function of position along the crawler and that the sliding stress ($\sigma_{sliding}$) is related to that as obtained from the sliding disc experiments:

$$\sigma_{sliding}(x,t) = f_{\pm}(x,t)v(x,t) \qquad \sigma_{sliding}(x,t) = f_{\pm}(x,t)v(x,t) \quad [4]$$

The normalized friction coefficients depend on the state of contraction that is found at position x along the crawler at time t and whether it is in the heating (+) or cooling (-) part of the cycle. Then by imposing that the total force on the crawler is zero, explicit expressions for $\frac{\partial x_0}{\partial \varepsilon}$ in eq [3] can be found in terms of the local contraction and friction coefficients. The local contraction of the crawler has been determined from the image analysis of video images of a crawler in action. With this information, the friction coefficient as a function of position along the crawler can be obtained. Subsequently, these expressions are solved numerically to yield the net displacement.

The dependence of the net displacement on the irradiation position is predicted quite well by the model (Fig 3B). In both the experiments and the theory, the irradiation position that leads to maximum displacement is found to be around 35% of the microcrawler length (Fig 3B). The model underpredicts the net displacement by at most a factor of two. The main reason for this difference is that the friction hysteresis values used in the calculation were acquired indirectly from the sliding experiment and may differ from the hysteresis loop in the crawling process.

Next, we used the data from sliding experiments in pluronic (Figure S8) for the model to predict net displacement of the crawler in the pluronic surfactant. The predicted displacement in such case dropped to maximum 2-3 μm per one stroke for all three crawlers (Figure S9). This trend corresponds to experimental findings (observed net displacement ~1-2 μm) and further supports our above-described explanation of crawling ultimately originating from the friction hysteresis.

Steerable Microcrawlers, Crawling up a slope, Fast actuation

The mechanism for crawling can be applied to various shapes such as discs, crosses, or 'Pac-man' shape microcrawlers (supplementary video S2). Regardless of the microcrawlers geometry, the displacement is always parallel to the line connecting the irradiation spot and the microcrawlers center of mass. Consequently, the direction of crawling can be controlled by the choice of the irradiation spot. To demonstrate controlled steering with translation and rotation control, we prepared a 'U' shaped microcrawler as depicted in Figure 4A. This steerable microcrawler can be perceived as two rectangular microcrawlers, described in previous sections, connected at the front end. Applying laser pulses to the back of one of these 'elemental' microcrawlers results in its forward motion, following a circular pathway. By alternating the pulsed irradiation of each ends of the U shaped microcrawler, it can be moved in a straight line; irradiation of only one end results in turning. This control mechanism resembles control over a tracked vehicle, where the speed of track on each side is controlled independently and used to control the direction of movement. We utilized this steerable microcrawler for the transport of hydrogel cubes (25 × 25 × 25 μm) by simply pushing them over the surface (Figure 4D, supplementary video S3). The microcrawler is steered to pick and gather the cubes at its front edge, the presence of small spikes at front corners prevents their loss. Several cubes can be pushed at a same time. Notably, no changes in the contraction-expansion behavior were detected upon hundreds of irradiations performed in this experiment, indicating no permanent damage to the hydrogel or leakage of entrapped gold particles.

Practical applications of a microcrawler may require navigation through complex, uneven environments. Therefore, we tested the ability of our microcrawler to climb up a slope. The tested 50

× 100 µm rectangular microcrawler managed to crawl up to 20° inclined slope. Figure 4C shows, that small tilt angles do not affect the net displacement length, which rapidly drops close to the limiting angle of 20°. The reason for the drop is a gravity-induced backward slide of a microcrawler, taking place simultaneously while crawling, at the limiting angle the velocity of the backward slide matches that of the forward crawling.

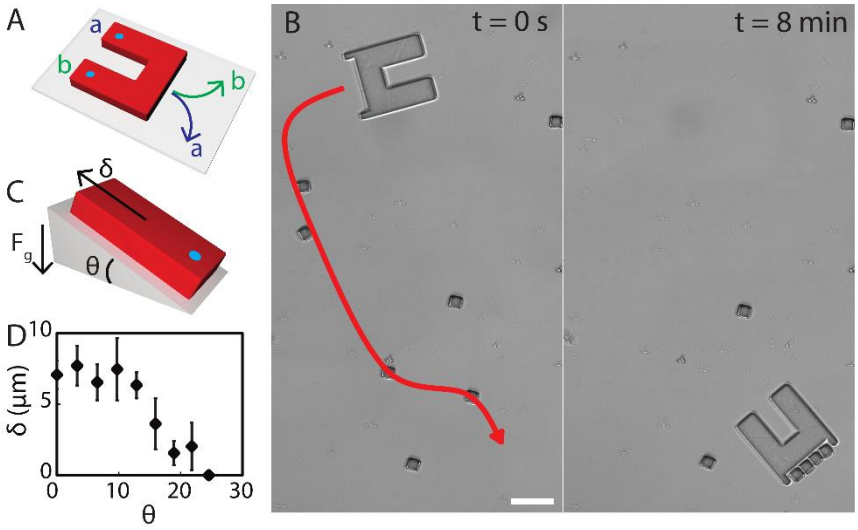

Figure 4. Steering and crawling uphill. A – 'U'-shaped crawler is steered by aiming the laser beam at spot a or b to turn right and left respectively. B – Steerable crawler is navigated and manipulates 25 µm hydrogel cubes. (scale bar corresponds to 100 µm). C – Cartoon of a crawler moving uphill. D – Plot of net displacement (δ) as a function of inclination angle (θ) for uphill crawling.

To test the maximum speeds of our microcrawlers, we applied higher frequency pulse sequences. As the frequency increases, the degree of contraction decreases and the hydrogel is not able to fully contract nor expand. Still, such actuation provided efficient forward motion. As an example, we show crawling by pulses as short as 25 ms, separated by 50 ms delays in between. The longer crawlers proved more efficient than the 100 µm crawler under high-frequency irradiation (Supplementary video S5 displays 180 µm long crawler). Although the total contraction (actuation amplitude) is only around 1.5 µm under these conditions, compared to a contraction of 40 µm under low-frequency irradiation, the displacement per cycle is 1.5 µm and 10-15 µm in low and high-frequency regime respectively. Under low-frequency irradiation, the step length is only 1/3 of the total contraction, whereas under high-frequency irradiation it is comparable to the total contraction during one cycle. The microcrawler speed at high-frequency irradiation is doubled, compared to the speeds observed at our nominal conditions and corresponds 18 µm per second (i.e. 0.1 body length per second). Following the microcrawlers with

the laser at these velocities proved difficult manually and so the recorded velocity could only be maintained only for several seconds, we are currently developing computer control of the irradiation.

Conclusion

In summary, we demonstrated a new locomotion principle of hydrogel microcrawlers, propelled remotely through light-induced reciprocal actuation, leveraging friction hysteresis between shrinkage and expansion phase of the cycle. The way our microcrawler leverages spatiotemporal modulation of friction mimics living crawlers, such as leech or inchworm, that can actively stick part of their body to the substrate for efficient crawling. This new mechanism enables the design of reciprocally actuating microcrawlers that can move uphill and manipulate other micro-objects. The microcrawler production is straightforward and scalable, owing to the continuous nature of stop-flow lithography.[42] The main drawback of our current design is the necessity of spatiotemporal modulation of light to achieve the directional motion. Our current research is focusing on overcoming this hurdle by synthesizing dual material microcrawlers with nonresponsive front side and actuating rear side, that crawl directionally when exposed to unfocused light pulses. The robustness of our mechanism principally allows for future changes of the power source (such as a chemical oscillator[15]) and subsequent construction of microrobots locomoting without the need for any external setup.

References

1. Sitti M, Ceylan H, Hu W, Giltinan J, Turan M, Yim S, Diller E. Biomedical Applications of Untethered Mobile Milli/Microrobots. Proc. IEEE. 2015;103(2):205–224.

2. Kim M. *Microbiorobotics: Biologically Inspired Microscale Robotic Systems*; Elsevier: Boston, MA, 2017.

3. Cianchetti M, Laschi C, Menciassi A, Dario P. Biomedical Applications of Soft Robotics. Nat. Rev. Mater. 2018;3(6):143–153.

4. Palagi S, Fischer P. Bioinspired Microrobots. Nat. Rev. Mater. 2018;3113–124.

5. Sitti M. Miniature Soft Robots — Road to the Clinic. Nat. Rev. Mater. 2018.

6. Tasoglu S, Diller E, Guven S, Sitti M, Demirci U. Untethered Micro-Robotic Coding of Three-Dimensional Material Composition. Nat. Commun. 2014;5.

7. Floyd S, Pawashe C, Sitti M. Two-Dimensional Contact and Noncontact Micromanipulation in Liquid Using an Untethered Mobile Magnetic Microrobot. IEEE Trans. Robot. 2009;25(6):1332–1342.

8. Shen T, Font MG, Jung S, Gabriel ML, Stoykovich MP, Vernerey FJ. Remotely Triggered Locomotion of Hydrogel Mag-Bots in Confined Spaces. Sci. Rep. 2017;7(1).

9. Loget G, Kuhn A. Electric Field-Induced Chemical Locomotion of Conducting Objects. Nat. Commun. 2011;2535.

10. Chen X-Z, Jang B, Ahmed D, Hu C, De Marco C, Hoop M, Mushtaq F, Nelson BJ, Pané S. Small-Scale Machines Driven by External Power Sources. Adv. Mater. 2018;30(15):1705061.

11. Lee H, Xia C, Fang NX. First Jump of Microgel; Actuation Speed Enhancement by Elastic Instability. Soft Matter. 2010;6(18):4342–4345.

12. Zeng H, Wasylczyk P, Parmeggiani C, Martella D, Burresi M, Wiersma DS. Light-Fueled Microscopic Walkers. Adv. Mater. 2015;27(26):3883–3887.

13. Rogóż M, Zeng H, Xuan C, Wiersma DS, Wasylczyk P. Light-Driven Soft Robot Mimics Caterpillar Locomotion in Natural Scale. Adv. Opt. Mater. 2016;4(11):1689–1694.

14. Morales D, Palleau E, Dickey MD, Velev OD. Electro-Actuated Hydrogel Walkers with Dual Responsive Legs. Soft Matter. 2014;10(9):1337–1348.

15. Maeda S, Hara Y, Sakai T, Yoshida R, Hashimoto S. Self-Walking Gel. Adv. Mater. 2007;19(21):3480–3484.

16. Hu W, Lum GZ, Mastrangeli M, Sitti M. Small-Scale Soft-Bodied Robot with Multimodal Locomotion. Nature. 2018;554(7690):81–85.

17. Palagi S, Mark AG, Reigh SY, Melde K, Qiu T, Zeng H, Parmeggiani C, Martella D, Sanchez-Castillo A, Kapernaum N, *et al.* Structured Light Enables Biomimetic Swimming and Versatile Locomotion of Photoresponsive Soft Microrobots. Nat. Mater. 2016;15(6):647–653.

18. Mourran A, Zhang H, Vinokur R, Möller M. Soft Microrobots Employing Nonequilibrium Actuation via Plasmonic Heating. Adv. Mater. 2017;29(2):n/a-n/a.

19. Alapan Y, Yasa O, Yigit B, Yasa IC, Erkoc P, Sitti M. Microrobotics and Microorganisms: Biohybrid Autonomous Cellular Robots. Annu. Rev. Control Robot. Auton. Syst. 2019;2(1):205–230.

20. Maeda S, Hara Y, Sakai T, Yoshida R, Hashimoto S. Self-Walking Gel. Adv. Mater. 2007;19(21):3480–3484.

21. Osada Y, Okuzaki H, Hori H. A Polymer Gel with Electrically Driven Motility. Nature. 1992;355(6357):242–244.

22. Zeng H, Wasylczyk P, Wiersma DS, Priimagi A. Light Robots: Bridging the Gap between Microrobotics and Photomechanics in Soft Materials. Adv. Mater. 2017;30(24):1703554.

23. Palagi S, Mark AG, Reigh SY, Melde K, Qiu T, Zeng H, Parmeggiani C, Martella D, Sanchez-Castillo A, Kapernaum N, *et al.* Structured Light Enables Biomimetic Swimming and Versatile Locomotion of Photoresponsive Soft Microrobots. Nat. Mater. 2016;15(6):647–653.

24. Zeng H, Wasylczyk P, Parmeggiani C, Martella D, Burresi M, Wiersma DS. Light-Fueled Microscopic Walkers. Adv. Mater. 2015;27(26):3883–3887.

25. Ohm C, Brehmer M, Zentel R. Liquid Crystalline Elastomers as Actuators and Sensors. Adv. Mater. 2010;22(31):3366–3387.

26. Sul OJ, Falvo MR, Taylor RM, Washburn S, Superfine R. Thermally Actuated Untethered Impact-Driven Locomotive Microdevices. Appl. Phys. Lett. 2006;89(20):203512.

27. Rogóż M, Zeng H, Xuan C, Wiersma DS, Wasylczyk P. Light-Driven Soft Robot Mimics Caterpillar Locomotion in Natural Scale. Adv. Opt. Mater. 2016;4(11):1689–1694.

28. Zeng H, Wani OM, Wasylczyk P, Priimagi A. Light-Driven, Caterpillar-Inspired Miniature Inching Robot. Macromol. Rapid Commun. 2018;39(1):1700224.

29. Camacho-Lopez M, Finkelmann H, Palffy-Muhoray P, Shelley M. Fast Liquid-Crystal Elastomer Swims into the Dark. Nat. Mater. 2004;3(5):307–310.

30. Zhu C-H, Lu Y, Peng J, Chen J-F, Yu S-H. Photothermally Sensitive Poly(N-Isopropylacrylamide)/Graphene Oxide Nanocomposite Hydrogels as Remote Light-Controlled Liquid Microvalves. Adv. Funct. Mater. 2012;22(19):4017–4022.

31. DeSimone A, Tatone A. Crawling Motility through the Analysis of Model Locomotors: Two Case Studies. Eur. Phys. J. E. 2012;35(9).

32. Eldering J, Jacobs H. The Role of Symmetry and Dissipation in Biolocomotion. SIAM J. Appl. Dyn. Syst. 2016;15(1):24–59.

33. Tung HW, Maffioli M, Frutiger DR, Sivaraman KM, Pané S, Nelson BJ. Polymer-Based Wireless Resonant Magnetic Microrobots. IEEE Trans. Robot. 2014;30(1):26–32.

34. Sul OJ, Falvo MR, Taylor RM, Washburn S, Superfine R. Thermally Actuated Untethered Impact-Driven Locomotive Microdevices. Appl. Phys. Lett. 2006;89(20):203512.

35. Purcell EM. Life at Low Reynolds Number. Am. J. Phys. 1977;45(1):3–11.

36. Lee K, Kim Y, Paik JK, Shin B. Clawed Miniature Inchworm Robot Driven by Electromagnetic Oscillatory Actuator. J. Bionic Eng. 2015;12(4):519–526.

37. Ueno S, Takemura K, Yokota S, Edamura K. Micro Inchworm Robot Using Electro-Conjugate Fluid. Sens. Actuators Phys. 2014;21636–42.

38. Plaut RH. Mathematical Model of Inchworm Locomotion. Int. J. Non-Linear Mech. 2015;7656–63.

39. Lu H, Zhu J, Lin Z, Guo Y. An Inchworm Mobile Robot Using Electromagnetic Linear Actuator. Mechatronics. 2009;19(7):1116–1125.

40. Yang C, Wang W, Yao C, Xie R, Ju X-J, Liu Z, Chu L-Y. Hydrogel Walkers with Electro-Driven Motility for Cargo Transport. Sci. Rep. 2015;513622.

41. Fairbanks BD, Schwartz MP, Bowman CN, Anseth KS. Photoinitiated Polymerization of PEG-Diacrylate with Lithium Phenyl-2,4,6-Trimethylbenzoylphosphinate: Polymerization Rate and Cytocompatibility. Biomaterials. 2009;30(35):6702–6707.

42. Dendukuri D, S. Gu S, C. Pregibon D, Alan Hatton T, S. Doyle P. Stop-Flow Lithography in a Microfluidic Device. Lab. Chip. 2007;7(7):818–828.

43. Behn C, Zeidis I, Zimmermann K. *Mechanics of Terrestrial Locomotion*; Springer Berlin Heidelberg: Berlin, Heidelberg, 2009.

44. Kreer T. Polymer-Brush Lubrication: A Review of Recent Theoretical Advances. Soft Matter. 2016;12(15):3479–3501.

45. Nalam PC, Ramakrishna SN, Espinosa-Marzal RM, Spencer ND. Exploring Lubrication Regimes at the Nanoscale: Nanotribological Characterization of Silica and Polymer Brushes in Viscous Solvents. Langmuir. 2013;29(32):10149–10158.

46. Kaneko Y, Yoshida R, Sakai K, Sakurai Y, Okano T. Temperature-Responsive Shrinking Kinetics of Poly (N-Isopropylacrylamide) Copolymer Gels with Hydrophilic and Hydrophobic Comonomers. J. Membr. Sci. 1995;101(1):13–22.

47. Morimoto N, Ohki T, Kurita K, Akiyoshi K. Thermo-Responsive Hydrogels with Nanodomains: Rapid Shrinking of a Nanogel-Crosslinking Hydrogel of Poly(N-Isopropyl Acrylamide). Macromol. Rapid Commun. 2008;29(8):672–676.

48. Liu G, Zhang G. Collapse and Swelling of Thermally Sensitive Poly(N-Isopropylacrylamide) Brushes Monitored with a Quartz Crystal Microbalance. J. Phys. Chem. B. 2005;109(2):743–747.

49. Cheng H, Liu G, Wang C, Zhang G, Wu C. Collapse and Swelling of Poly(N-Isopropylacrylamide-Co-Sodium Acrylate) Copolymer Brushes Grafted on a Flat SiO2 Surface. J. Polym. Sci. Part B Polym. Phys. 2006;44(4):770–778.

50. Cheng H, Shen L, Wu C. LLS and FTIR Studies on the Hysteresis in Association and Dissociation of Poly(N-Isopropylacrylamide) Chains in Water. Macromolecules. 2006;39(6):2325–2329.

51. Lu Y, Zhou K, Ding Y, Zhang G, Wu C. Origin of Hysteresis Observed in Association and Dissociation of Polymer Chains in Water. Phys. Chem. Chem. Phys. 2010;12(13):3188.

52. Varma S, Bureau L, Débarre D. The Conformation of Thermoresponsive Polymer Brushes Probed by Optical Reflectivity. Langmuir. 2016;32(13):3152–3163.

53. de Beer S. Switchable Friction Using Contacts of Stimulus-Responsive and Nonresponding Swollen Polymer Brushes. Langmuir. 2014;30(27):8085–8090.

54. Singh MK, Ilg P, Espinosa-Marzal RM, Kröger M, Spencer ND. Polymer Brushes under Shear: Molecular Dynamics Simulations Compared to Experiments. Langmuir. 2015;31(16):4798–4805.

55. Essö C. *Modifying Polydimethylsiloxane (PDMS) Surfaces*; Institutionen för biologi och kemiteknik, 2007.

56. Lee S, Iten R, Müller M, Spencer ND. Influence of Molecular Architecture on the Adsorption of Poly(Ethylene Oxide)−Poly(Propylene Oxide)−Poly(Ethylene Oxide) on PDMS Surfaces and Implications for Aqueous Lubrication. Macromolecules. 2004;37(22):8349–8356.